Inertial Measurement Units:
Modeling & Calibration

Tolga Özaslan [1]

Abstract

Inertial Measurement Units (IMUs) consist of various sensors, including accelerometers, gyroscopes, and magnetometers. Depending on the design choices of the manufacturer, an IMU may integrate one or more of these sensors, often incorporating multiple units to provide redundancy and enhance reliability. These sensors generate high-frequency data, typically ranging from 100 Hz to 1000 Hz, making them significantly faster than alternative perception sensors such as cameras, LiDARs, and depth sensors commonly employed in mobile robotics. Due to their high update rates and acceptable error bounds, IMUs are the primary choice for short-term state estimation. In particular, within the Kalman filter framework—widely implemented across mobile robotic systems—the process update step is driven by measurements obtained from accelerometers and gyroscopes. Consequently, IMUs are indispensable in mobile robotics applications. However, these sensors inherently exhibit noise and biases, which can lead to unreliable outputs if not properly calibrated or employed alongside appropriate mathematical filtering techniques, such as the Kalman filter family. This work provides a comprehensive analysis of IMUs and their constituent sensors, examining their working principles, sources of noise, calibration models, limitations, and strengths.

1   INTRODUCTION

Mobile robotics applications, including autonomous aerial drones (Özaslan et al., 2017), self-navigating ground vehicles , underwater platforms (Ioannou et al., 2024), and even rockets, extensively rely on accelerometers, gyroscopes, and magnetometers for state estimation and motion tracking. Depending on the specific application requirements, these platforms may integrate redundant sensor configurations, incorporating multiple instances of one or more of these sensors to enhance reliability and accuracy (Meier, Tanskanen, Fraundorfer, &

[1]Dr. Öğr. Üyesi, Ankara Yıldırım Beyazıt Üniversitesi, Mühendislik ve Doğa Bilimleri Fakültesi, 06010, Ankara, Türkiye, ORCID: 0000-0002-5002-0670, E-posta: tozaslan@aybu.edu.tr

Pollefeys, 2011). Such sensor assemblies are typically encapsulated within a single unit known as an Inertial Measurement Unit (IMU).

An IMU integrates multiple sensors to provide precise motion and orientation data. The accelerometer measures linear acceleration, enabling the estimation of external forces—such as aerodynamic drag and external perturbations—when the mass of the system is known. Additionally, the accelerometer facilitates tilt estimation by detecting the direction of the gravitational field, thereby enabling movement detection and orientation changes relative to the inertial frame (Freescale, 2013). The gyroscope measures angular velocity and orientation within the IMU's frame, allowing for accurate tracking of rotational motion (Kraft, 2003). Unlike accelerometers, gyroscopes do not measure a reference vector, such as gravity. However, by integrating gyroscope measurements over time, orientation can be estimated with high precision. The magnetometer, often referred to as a digital compass, detects Earth's magnetic field as well as other magnetic sources in the environment, assisting in absolute heading estimation, provided that magnetic disturbances are minimal.

Each of these sensors exhibits inherent strengths and limitations. However, when properly calibrated and fused within an appropriate estimation framework, their complementary characteristics compensate for individual weaknesses (Fong, Ong, & Nee, 2008; Rehder, Nikolic, Schneider, Hinzmann, & Siegwart, 2016; Tedaldi, Pretto, & Menegatti, 2014). By leveraging sensor fusion techniques, an IMU enables accurate estimation of position, velocity, and attitude, making it an indispensable component in robotics, drone navigation, aerospace systems, and mobile devices.

1.1 Misconceptions about IMUs

When examining manufacturer catalogs or technical documentation, various naming conventions and descriptions regarding the capabilities of IMUs can lead to misconceptions. One common misunderstanding pertains to the specific functionalities of different sensors within an IMU. Many users are uncertain about the role of accelerometers, gyroscopes, and magnetometers, their respective strengths and limitations, and the types of devices that incorporate IMUs, such as smartphones (Michel, Geneves, Fourati, & Layaida, 2017), automobiles, drones, and aircraft.

IMUs may contain 1-axis, 2-axis, or 3-axis configurations of accelerometers, gyroscopes, and magnetometers (each), typically arranged perpendicularly to one another. This configuration has led to confusion in terminology, particularly regarding sensor nomenclature. For instance, terms such as *6-axis accelerometer* or *6-axis gyroscope* are technically inaccurate and misleading. In contrast, the designation *9-axis IMU* correctly refers to an IMU that integrates a 3-axis accelerometer, a 3-axis gyroscope, and a 3-axis magnetometer.

Another prevalent misconception involves the concept of degrees of freedom (DoF) in relation to IMUs. IMUs themselves do not possess intrinsic degrees of freedom; rather, they provide sensor data that facilitates the estimation of a platform's state within its degrees of freedom. A rigid body operating in three-dimensional space inherently exhibits six degrees of freedom—three translational and three rotational. Therefore, marketing claims suggesting that an IMU can estimate *9 DoF* are misleading. A more precise statement would be that *the IMU enables the estimation of the full six degrees of freedom of a platform, potentially incorporating additional sensor fusion techniques for improved state estimation*. Knowledgeable vendors and manufacturers should adhere to accurate terminology to avoid propagating misconceptions regarding IMU capabilities.

1.2   The Sudden Rise of IMUs in the Market

The accessibility of IMUs significantly improved after the U.S. Department of Motor Vehicles (DMV) mandated the installation of airbags in all new cars. Airbags rely on accelerometers to detect sudden deceleration and trigger deployment, leading major manufacturers such as Bosch, STMicroelectronics, and Analog Devices to invest heavily in MEMS (Micro-Electro-Mechanical Systems) technology. This investment drove mass production, reducing costs and making IMUs more accessible to researchers and consumer electronics manufacturers. As a result, IMUs became widely adopted in robotics, navigation, and entertainment applications (Figure 1).

With increased accessibility, IMUs quickly became essential in various fields due to their ability to provide real-time motion and orientation data. In inertial navigation, IMUs are crucial for aircraft and missiles, enabling precise positioning without relying on external references. For state estimation, IMUs

Figure 1: Application areas of IMUs include game consoles, virtual and augmented reality, inertial navigation and missile guidance systems.

help drones and autonomous ground vehicles maintain stability and accurately track motion. In attitude control applications, IMUs support VTOL drones by facilitating self-balancing, flipping maneuvers, and enhancing the agility of racing drones. In virtual and augmented reality, devices like the Oculus (LaValle, Yershova, Katsev, & Antonov, 2014) headset utilize IMUs to track head movements, improving immersion and user experience. Similarly, gaming consoles such as the Nintendo Wii integrate IMUs to detect user motion, enabling interactive gameplay. The widespread adoption of IMUs in these domains underscores their versatility and importance in modern technology.

1.3 Review on Orientation Estimation

Orientation estimation using IMUs has been a significant focus in academic research, initially driven by satellite control applications (Black, 1964). Early methods relied on magnetometers to determine orientation relative to Earth's magnetic field. NASA played a key role in advancing orientation representation over the years (Bar-Itzhack, 2000). In particular the Eulerian approach, requiring extensive trigonometric computations, was deemed impractical due to the computational limitations of early processors.

As the demand for efficient attitude estimation grew, quaternion algebra gained prominence for its compact, singularity-free representation of rotations, making it ideal for spacecraft and robotics (Dantam, 2002; Eberly, 2002; Katthöfer & Yoon, 2012). Researchers like (Hartley, Trumpf, Dai, & Li, 2013; Markley, Cheng, Crassidis, & Oshman, 2007; Valenti, Dryanovski, & Xiao, 2015) contributed to quaternion averaging, crucial for spacecraft attitude estimation and multi-sensor fusion.

Gyroscopes and their companion sensors are essential for attitude estimation in IMUs, but they are inherently noisy. Proper noise modeling such as the work (Lam, Stamatakos, Woodruff, & Ashton, 2003) is crucial for integration into estimators like the Extended or Unscented Kalman Filter to achieve accurate results (Guo, Wu, Wang, & Qian, 2017).

Early orientation estimation methods relied on complementary filters to fuse accelerometer and gyroscope data. A major improvement came with nonlinear complementary filters, introduced in (Mahony, Hamel, & Pflimlin, 2005), offering a robust attitude estimation framework. This approach was further refined by (Mahony, Hamel, & Pflimlin, 2008) and (Hamel & Mahony, 2006), who formulated it on the special orthogonal group $SO(3)$, improving stability and computational efficiency. (Huynh, 2009) proposed a method for defining distances between orientations which also helped in defining filtering techniques.

To address gyro bias drift, (Euston, Coote, Mahony, Kim, & Hamel, 2008) extended the passive complementary filter with an adaptive mechanism, enhancing long-term accuracy—especially for UAV applications. Also Kalman filters add the bias terms to their state vectors to update the noise model parameters on-the-file (Sun et al., 2018)

One of the more recent filters for orientation estimation is the Madgwick filter (Madgwick, 2010), which offers several advantages over the Kalman family of filters (Hartikainen, Solin, & Särkkä, 2011), including lower computational complexity, no need for matrix inversion, and reduced latency, making it well-suited for real-time applications. Similarly, (Fourati, Manamanni, Afilal, & Handrich, 2011) proposed a nonlinear filtering approach based on the Levenberg-Marquardt algorithm to enhance orientation estimation using low-cost IMUs. Similar to Madgwick's work (Liu, Liu, Gong, & Wu, 2018) proposed a fast estimator based on a Kalman filter.

The range of orientation estimation, IMU calibration, and filtering approaches is extensive. The references provided serve as a starting point for a more in-depth exploration of the topic. Given the vast number of available methods, a comprehensive listing is beyond the scope of this work.

2 WORKING PRINCIPLE OF MEMS SENSORS

In this section, we examine the fundamental components of a typical IMU, namely the MEMS accelerometer, gyroscope, and magnetometer. These sensors are fabricated using micro-electromechanical systems (MEMS) technology and are often smaller than a fraction of a millimeter.

To provide a sense of scale, one can refer to the technical specifications of widely used models such as ADXL345 by Analog Devices, MPU6050 by InvenSense/TDK or L3GD20H by STM. Due to mass production, these sensors are relatively inexpensive, typically costing around $2-5. However, when integrated into high-end IMUs that incorporate real-time thermal calibration, signal filtering, and state estimation, their cost can increase significantly, reaching hundreds of USD, as seen in models of manufacturers such as VectorNav, MicroStrain.

2.1 MEMS Accelerometers

2.1.1 Working Principle

MEMS accelerometers function based on a mass-spring system within a microfabricated structure. A simplified schematic of a typical MEMS accelerometer is shown in Figure 2. The sensor consists of a *proof mass* (the ball at the center) suspended by springs within the device envelope. External forces, whether from the gravitational field or the motion of the sensor, cause the mass to displace, leading to deformation of the springs.

If the displacement is due to gravity, the proof mass moves in the same direction as the gravitational acceleration vector. Conversely, if the force is induced by motion, the mass deflects opposite to the acceleration vector relative to the sensor envelope. By measuring the deformation of the springs, the force acting on the mass can be determined, allowing for the estimation of acceleration. This principle forms the basis of MEMS accelerometers used in modern devices.

Figure 2 illustrates different cases of accelerometer behavior. In Figure 2-a, the sensor is neither accelerating nor subjected to a gravitational field, which may occur if the gravity vector is perpendicular to the sensor's sensing plane. In
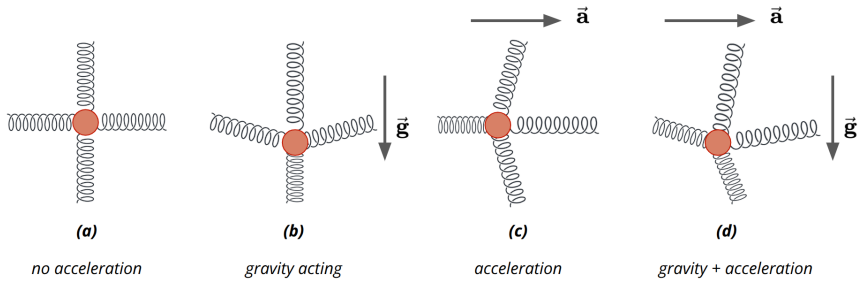
Figure 2: A model for a MEMS accelerometer. A mass is connected to the sensor body through springs. Changes in spring length are converted into acceleration.

Figure 2-b, the sensor is in a gravitational field, causing the proof mass to deflect in the same direction as the gravitational acceleration. Figure 2-c depicts a scenario where the sensor is accelerating to the right without gravitational influence, or where the gravitational field is perpendicular to the motion plane of the mass. The rightmost figure represents a case where the sensor experiences both acceleration and gravity simultaneously.

As can be observed, the sensor cannot inherently distinguish between proof mass deflection caused by gravity or motion. Both effects result in identical measurements. For instance, in Figure 2-b, the sensor may falsely interpret its stationary state under gravity as an upward acceleration.

This static deflection due to gravity can either be a challenge or a useful reference for orientation estimation, depending on the application. For example, when a drone flies against a drag force, the accelerometer captures both the external force and gravitational influence. Extracting motion-induced components from raw sensor data requires advanced filtering techniques. However, when the sensor is at rest or moving at constant velocity with no external forces, its raw accelerometer readings (excluding sensor noise) directly correspond to the gravitational vector. As discussed in the following sections, this property enables reliable estimation of roll and pitch angles—collectively known as tilt angles.
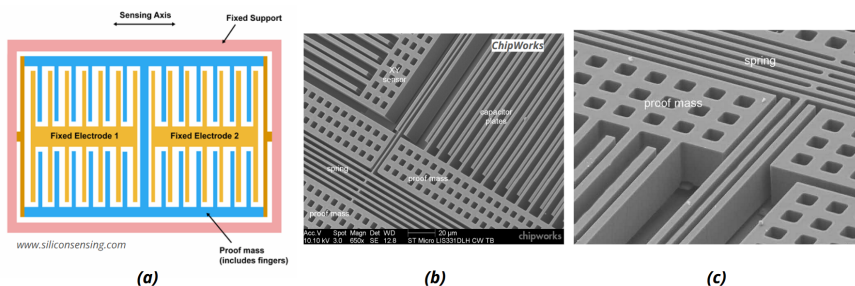
Figure 3: (a) Schematic illustration of a single-axis MEMS accelerometer. (b-c) Electron microscope images of a MEMS accelerometer, showing the proof mass and comb-like electrode structures.

2.1.2 Electro-Mechanical Structure

MEMS accelerometers are a type of micro-electromechanical system (MEMS) fabricated using microelectronic manufacturing techniques. They primarily operate based on capacitive sensing, which is the most common method, or piezoresistive sensing. A schematic representation of a MEMS accelerometer, along with an electron microscope image of an actual device, is shown in Figure 3.

The figure illustrates the internal structure of a MEMS accelerometer, highlighting the proof mass, suspension springs, and capacitor plates that enable sensing. These components function together to detect acceleration changes and provide precise motion measurements for various applications.

At the core of a MEMS accelerometer is a proof mass suspended within the structure by flexible springs (Figure 3-b). When an external force is applied, the proof mass resists motion due to inertia, causing a relative displacement within its enclosure. This displacement alters the capacitance between adjacent comb-like electrode structures, which is then measured and converted into an acceleration value.

Comb-like structured MEMS accelerometers operate based on the relative motion of interdigitated capacitor plates. Since these plates are extremely thin, they effectively behave as capacitors. As the moving comb structure shifts due to acceleration, the capacitance between adjacent plates changes. This variation in capacitance induces a voltage difference across the plates, which is then used to infer the displacement of the proof mass relative to the sensor envelope
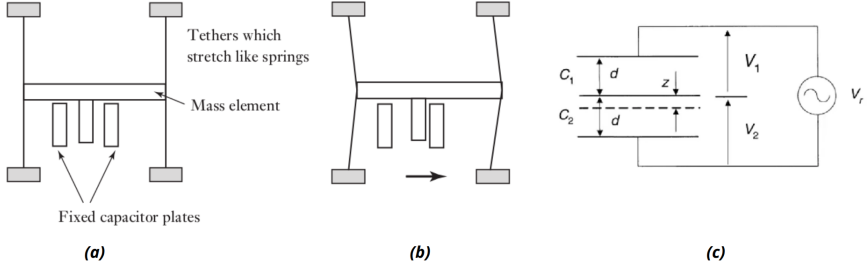
Figure 4: (a) Fixed and moving capacitor plates. (b) Gap between capacitor plates change as the sensor accelerates. (c) Voltage difference accross the plates is measured to infer proff-mass displacement (Bolton, 2003).

(Figure 4). The relationship between capacitance and displacement is given by:

$$C - \Delta C = \varepsilon_r \varepsilon_0 \frac{A}{d+z} \quad \rightarrow \quad \frac{\Delta C}{C} = -\frac{x/d}{1+(z/d)} \tag{1}$$
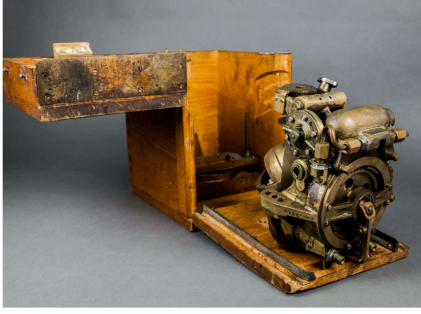
where C is the initial capacitance between the plates, ΔC is the change in capacitance due to displacement, d is the initial separation between the capacitor plates, z is the displacement of the proof mass, x is the total displacement of the sensing element relative to the sensor frame, and $\varepsilon_r, \varepsilon_0$ are constants.

As evident from these equations, the relationship between displacement (z) and capacitance (ΔC) is nonlinear, which can introduce complexity in signal processing. A more effective approach is to use a differential capacitance configuration, which establishes a linear relationship between displacement and voltage difference (Figure 4-c). The differential capacitance equations are derived as:
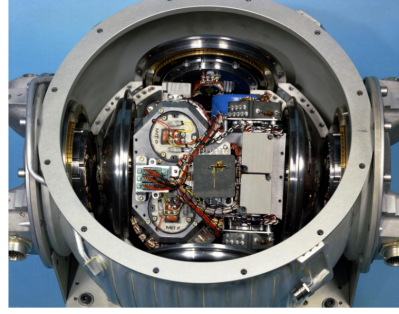
$$V_1 = V_r \frac{C_2}{C_1 + C_2} \quad , \quad V_2 = V_r \frac{C_1}{C_1 + C_2} \quad \rightarrow \quad V_1 - V_2 = \frac{C_2 - C_1}{C_1 + C_2} \tag{2}$$

Plugging in capacitance expressions

$$C_1 = \varepsilon_0 \varepsilon_r \frac{A}{d-z}, \quad C_2 = \varepsilon_0 \varepsilon_r \frac{A}{d+z} \tag{3}$$

Figure 5: Examples of mechanical gyroscopes that were engineering marvels of their time.

we get

$$V_1 - V_2 = V_r \left(\frac{1/(d-z) - 1/(d+z)}{1/(d-z) + 1/(d+z)} \right) = V_r \frac{z}{d} \qquad (4)$$

Using the configuration in Figure 4-c, the voltage difference across the two capacitors is directly proportional to the displacement of the proof mass as shown above.

2.2 Gyroscope

2.2.1 Working Principle

A gyroscope is a device that exploits the gyroscopic effect, which is the resistance of a rotating mass to changes in its axis of rotation. This effect arises due to the conservation of angular momentum and is used to measure angular momentum.

Gyroscopes play a critical role in navigation and orientation determination in various applications. They are essential components in ships, aircraft, missiles, drones, submarines, torpedoes, and even spacecraft. Historical examples include the Japanese Type 93 "Long Lance" torpedo gyroscope, which was used in naval warfare. Modern implementations include the IMUs used in the Apollo navigation system for space exploration (Figure 5).

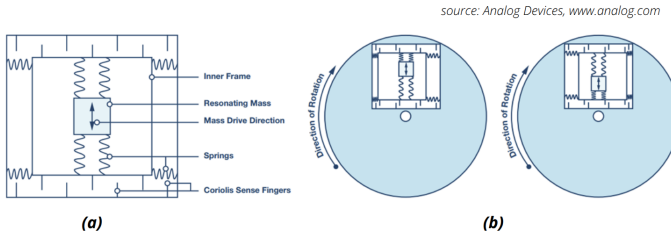Mechanical gyroscopes, while once engineering marvels, are bulky, heavy,

Figure 6: (a) A radially oscillating mass is supported by springs on both sides. (b) When the system undergoes rotation, Coriolis forces induce lateral displacement of the mass. *(Image source: Analog Devices)*

and require significant energy to sustain their angular momentum. In contrast, modern gyroscopes are designed and manufactured using MEMS technology, making them compact, lightweight, and energy-efficient.

MEMS gyroscopes operate based on the Coriolis effect, which arises when a vibrating structure experiences a change in its plane of motion. Instead of using a traditional spinning mass like mechanical gyroscopes, MEMS gyroscopes rely on vibrating elements that oscillate in a fixed plane. Figure 6 illustrate the working principle of these devices.

In Figure 6-a, the resonating mass oscillates radially at a controlled frequency. When the system rotates about an axis not parallel to the plane of oscillation, Coriolis forces cause lateral displacement of the mass, as shown in Figure 6-b. This displacement affects the lateral springs, leading to a measurable change in capacitance, similar to the sensing mechanism in MEMS accelerometers. Capacitive sense fingers detect these displacements by measuring differential capacitance between the moving mass and fixed electrodes. The resulting differential capacitance is converted into an electrical signal, which is proportional to the Coriolis force. Since the resonance frequency is known and actively controlled, the system can accurately derive the angular velocity around the axis perpendicular to the oscillation plane.

A similar principle is observed in nature, particularly in flying insects such as flies as shown in Figure 7. Insects possess specialized organs called *halteres*, which are small, club-shaped structures that oscillate in sync with wingbeats. As the insect changes direction during flight, the Coriolis forces acting on the halteres provide sensory feedback, enabling the insect to maintain stability and orientation. MEMS gyroscopes mimic this biological mechanism,

Figure 7: Flying insects are equipped with special organs called *halteres*, which help them control their orientation.

using vibrating structures to detect rotational movement and provide precise inertial measurements. This approach allows for compact, low-power, and cost-effective gyroscopes, making them ideal for modern applications in navigation, robotics, and consumer electronics.

2.2.2 Electro-Mechanical Structure

At the heart of a MEMS gyroscope lies a proof mass that is driven into oscillatory motion within a fixed plane (Figure 8). This motion is typically sustained at a resonant frequency using electrostatic actuation, which minimizes power consumption and enhances sensitivity.

Let's assume that the mass resonating along *X* axis. When the sensor undergoes rotation about the perpendicular axis (e.g. the *Z*-axis), the *Coriolis force* acts on the vibrating mass, causing a displacement along the third axis (e.g. the *Y*-axis). This force is given by:

$$F_c = 2mv\Omega_z \tag{5}$$

where F_c is the Coriolis force, m is the mass of the resonating element, v is the radial velocity of the vibrating mass, Ω_z is the angular velocity of the gyroscope.

The Coriolis force introduces a small displacement in the proof mass, which is then detected using capacitive sensing (Figure 6). Since this displacement is proportional to the angular velocity Ω_z, the system can reliably estimate
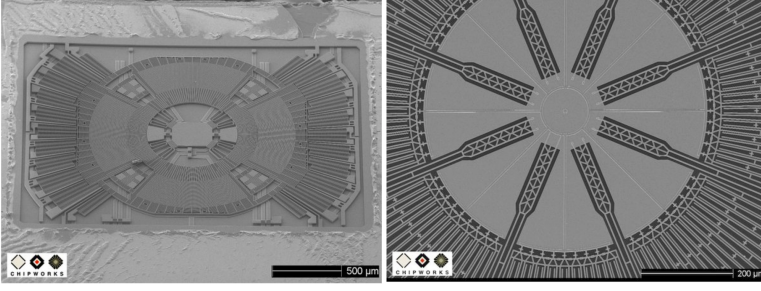
Figure 8: Close-up view of a MEMS gyroscope from an iPhone 4, highlighting its resonating structure. The circular pattern of the structure is clearly visible. *(Image source: ChipWorks)*

rotational motion. Solving for Ω_z in the above equation, we obtain:

$$\Omega_z = \frac{F_c}{2mv}.$$

(6)

Since the resonance frequency and proof mass are known system parameters, the measured Coriolis force can be used to accurately determine the angular velocity. The displacement caused by the Coriolis force is typically measured using differential capacitive sensing, employing a structure similar to that of accelerometers.

Finally, by arranging multiple gyroscopes along different axes, it is possible to infer rotational speed in multiple directions. This enables precise orientation estimation regardless of the mounting orientation of the gyroscopes on a mobile platform.

3 SENSOR MODEL

IMU calibration refers to the process of modeling the relationship between actual external excitations and the measurements provided by the IMU (Greenheck, 2015). Specifically, we focus on calibrating the accelerometer and gyroscope, as both sensors are subject to similar sources of error and noise, albeit with some differences due to their distinct operating principles.

As discussed in previous sections, both motion and gravity effect sensor outputs. Before acceleration or angular velocity measurements are obtained, the

sensor signals undergo multiple transformations, introducing noise due to electrical imperfections. Additionally, the mechanical structure of the sensors can introduce errors, such as manufacturing inaccuracies, misalignment of sensor axes, and structural inconsistencies. Proper calibration is essential to mitigate these effects and improve measurement accuracy.

The sources of error in IMU measurements can generally be categorized into two main groups: (1) Deterministic errors, (2) Stochastic errors. These errors affect both accelerometers and gyroscopes, impacting the accuracy and reliability of the measurements. In the following sections, we will examine each type of error in detail, discussing their origins and potential mitigation strategies.

3.1 Deterministic Errors

3.1.1 Static Bias

Static bias *might be* one of the most critical sources of error in IMUs, as it is typically additive in nature. This bias can vary with temperature fluctuations and power cycles, leading to drift in sensor readings over time. After each power cycle, the bias may change, and depending on temperature and electrical conditions, it can further drift, necessitating continuous recalibration.

In MAV applications, this error is often incorporated into the platform's state and updated dynamically within a Kalman filter framework (Özaslan et al., 2017; Sun et al., 2018). The bias error vector is expressed as:

$$\boldsymbol{b}_a^\top = \begin{bmatrix} b_{a,x} & b_{a,y} & b_{a,z} \end{bmatrix} \tag{7}$$

Bias errors introduce a constant offset in sensor measurements, affecting overall accuracy. To mitigate their impact, proper calibration and compensation techniques must be employed, ensuring reliable state estimation and control.

3.1.2 Scaling Factors

The raw measurements can be scaled up or down, distorting the actual values (Figure 9-a). When combined with additive bias errors, this scaling effect is typically sufficient to compensate for single-axis errors. For 3-axis accelerom-
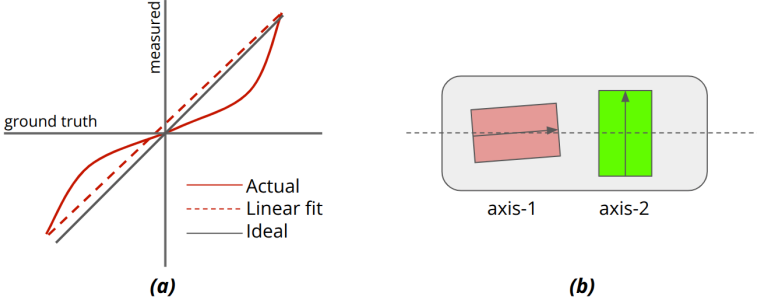
Figure 9: (a) Distortion of the ground truth acceleration/angular rate due to a non-unity scaling factor. (b) Multi-axis sensor with one of the single-axis components mounted with a slight misalignment.

eters and gyroscopes, the scaling factor can be modeled as a diagonal matrix, given by:

$$\mathbf{S}_a = \begin{bmatrix} S_{a,x} & 0 & 0 \\ 0 & S_{a,y} & 0 \\ 0 & 0 & S_{a,z} \end{bmatrix} \tag{8}$$

Ideally, $\mathbf{S}_a$ is the identity matrix.

3.1.3 Misalignment

Multiple single-axis sensors are integrated into a single package to form a 3-axis sensor. During the manufacturing process, individual single-axis sensors might be mounted onto the sensor base with slight misalignment. Although each sensor may provide accurate measurements individually, collectively, the sensor data can exhibit errors due to these misalignments (Figure 9-b). This misalignment is modeled using a 3×3 skew-symmetric matrix $\mathbf{M}_a$, which can be expressed as:

$$\mathbf{M}_a = \begin{bmatrix} 0 & M_{a,xy} & M_{a,xz} \\ -M_{a,xy} & 0 & M_{a,yz} \\ -M_{a,xz} & -M_{a,yz} & 0 \end{bmatrix} \tag{9}$$

Here, $M_{a,ij}$ represents the acceleration along axis j, as measured by sensor i.

3.1.4   g-Sensitivity *(Gyroscope Only)*

A gyroscope is ideally designed to measure angular rate. However, in practice, linear acceleration can influence the angular rate measurements. This occurs due to imperfections in the gyroscope's mechanical structure, causing it to exhibit unintended sensitivity to linear acceleration. As a result, the gyroscope bias shifts when subjected to translational acceleration. This effect is modeled by a full 3×3 matrix, denoted as the g-sensitivity matrix:

$$\boldsymbol{G}_g = \begin{bmatrix} G_{g,xx} & G_{g,xy} & G_{g,xz} \\ G_{g,yx} & G_{g,yy} & G_{g,yz} \\ G_{g,zx} & G_{g,zy} & G_{g,zz} \end{bmatrix} \tag{10}$$

The resulting error is computed as $\boldsymbol{e}_g = \boldsymbol{G}_g \boldsymbol{a}$ where $\boldsymbol{a}$ represents the actual translational acceleration of the sensor.

3.1.5   Temperature-Dependent Bias

The intricate structures inside a MEMS sensor are affected by temperature variations. Changes in material properties due to temperature fluctuations alter the mechanical response of spring structures, as explained in previous sections. This, in turn, impacts the sensor's measurement accuracy.

To mitigate this error, a lookup table (LUT) approach is commonly used. The sensor undergoes calibration at various temperature levels, and the corresponding correction parameters are stored. An internal temperature sensor continuously monitors the temperature and retrieves the most suitable calibration parameters from the LUT to compensate for temperature-induced biases.

3.2   Stochastic Errors

In the previous sections, we discussed various sources of deterministic errors that can be modeled to some extent. For example, additive bias can be estimated and subtracted from raw measurements, improving measurement accuracy. Since this bias persists over time with gradual fluctuations, it can be tracked using estimation techniques such as Kalman filtering. Similar modeling approaches apply to scaling errors, temperature-induced variations, and
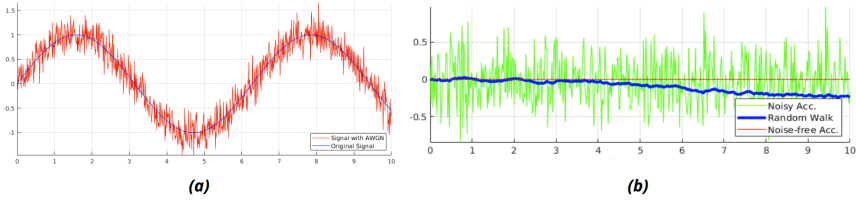
Figure 10: (a) Random noise superimposed on ground truth measurements. (b) Integration of random noise over time causing random walk in speed estimates.

misalignment errors.

However, there exist other sources of error that cannot be precisely determined and must instead be characterized using probability distributions. Unlike deterministic errors, these stochastic errors exhibit statistical properties, typically following Gaussian or Gamma distributions, but their individual values cannot be estimated with practically useful accuracy. These errors are categorized under stochastic noise models.

3.2.1 Random Noise

Random noise arises from thermo-mechanical fluctuations within the sensor. It is typically modeled as additive white Gaussian noise (AWGN) with the following zero-mean assumption. For gyroscopes, this type of noise is quantified as *Angle Random Walk (ARW)*, while for accelerometers, it is referred to as *Velocity Random Walk (VRW)* (Figure 10-a).

3.2.2 Bias Random Walk

Bias random walk is caused by electronic flicker noise, leading to random variations in the bias term even when external conditions, such as temperature, remain constant. Unlike deterministic bias errors, which can be corrected through calibration, bias random walk introduces long-term drift that requires continuous estimation (Figure 10-b).

To mitigate this effect, bias terms are typically included as part of an extended Kalman filter (EKF) or unscented Kalman filter (UKF) framework, allowing for dynamic compensation over time.

3.3 Mathematical Representations

3.3.1 Accelerometer Sensor Model

The sources of error for accelerometers can be categorized into deterministic and stochastic errors. Deterministic errors include static bias, scaling error, misalignment error, and temperature effects. These errors can often be modeled and compensated for through calibration. On the other hand, stochastic errors, such as white noise and random walk, cannot be precisely determined and are typically modeled using probabilistic methods.

The cumulative effect of these error sources can be expressed as:

$$K_a \tilde{a} = (\mathbf{I} + S_a + M_a)a + b_a + T_a \Delta T + \eta_a + \varepsilon_a \tag{11}$$

where K_a represents the sensitivity scale factor in units of g, and $\tilde{a}$ is the digital output of the accelerometer. The term $\mathbf{I}$ is the identity matrix, while S_a represents the scale factor matrix and M_a accounts for the skew-symmetric cross-coupling effects. The bias error is denoted as b_a, and $T_a \Delta T$ models the temperature-dependent variations in the measurements. The term η_a represents zero-mean white noise, while ε_a accounts for the random walk noise affecting the sensor output.

3.3.2 Gyroscope Sensor Model

The sources of error for gyroscopes are the same as those for accelerometers, with the addition of g-sensitivity, which accounts for the influence of linear acceleration on angular rate measurements. The combined effect of these error sources can be expressed as:

$$K_g \tilde{\omega} = (\mathbf{I} + S_g + M_g)\omega + b_g + G_g a + T_g \Delta T + \eta_g + \varepsilon_g \tag{12}$$

where K_g represents the sensitivity scale factor in units of *rad/sec*, and $\tilde{\omega}$ is the digital output of the gyroscope. The g-sensitivity matrix G_g introduces an error dependent on the acceleration input a. All other terms are similar to their counterparts in the accelerometer model.

3.4 Simplified Sensor Models

In certain scenarios, many of the terms included in the comprehensive sensor models (Equation 11-12) have either an insignificant effect on the measurements or are irrelevant due to the absence of specific factors in the application. For instance, if an IMU operates in a stable thermal environment with minimal temperature fluctuations, temperature-dependent error terms can be disregarded. Similarly, if the manufacturer employs high-precision assembly techniques, misalignment errors may be negligible. Additionally, if the IMU is not subjected to extreme accelerations, such as in missile guidance systems, the g-sensitivity term may have little impact. In such cases, the sensor models can be simplified by removing unnecessary terms while preserving essential measurement characteristics.

A simplified accelerometer model assumes that the measured acceleration is affected primarily by bias and Gaussian noise. This can be expressed as:

$$\tilde{\boldsymbol{a}} = \boldsymbol{a} + \boldsymbol{b}_a + \eta_a \tag{13}$$

where $\tilde{\boldsymbol{a}}$ represents the measured acceleration, $\boldsymbol{a}$ is the true acceleration, $\boldsymbol{b}_a$ accounts for the accelerometer bias, and η_a is zero-mean Gaussian noise with covariance Σ_a^2.

Similarly, the gyroscope model can be simplified using the same approach:

$$\tilde{\boldsymbol{\omega}} = \boldsymbol{\omega} + \boldsymbol{b}_g + \eta_g \tag{14}$$

where $\tilde{\boldsymbol{\omega}}$ is the measured angular velocity, $\boldsymbol{\omega}$ represents the true angular velocity, $\boldsymbol{b}_g$ accounts for gyroscope bias, and η_g is zero-mean Gaussian noise with covariance Σ_g^2.

These simplified models offer an effective means of interpreting IMU measurements, especially in applications where precise calibration is not feasible or necessary. By focusing on the dominant error sources while ignoring negligible effects, these models provide a balance between accuracy and computational efficiency.

4 SENSOR CALIBRATION

Calibration of an IMU can be performed using either professional calibration setups or simplified procedures based on well-defined conditions. A basic approach involves placing the sensor in known static orientations, such as resting on a table, and maintaining it stationary for a certain duration to collect reference measurements.

For high-end commercial products or military-grade devices, professional calibration setups are required to achieve precise and repeatable results. In such cases, a *tumble test* must be conducted (Figure 11). This test is specifically used to collect accelerometer data by placing the IMU on each of its faces or using a turntable. The objective is to ensure that the recorded measurements correspond to expected values, typically $\pm 1g$, in response to the gravitational field.

Gyroscope calibration, on the other hand, is typically performed using a *turntable*, where a constant angular velocity is applied about each axis to determine the sensor's scale factor and bias. The equipment commonly used for IMU calibration is illustrated in Figure 11.

The calibration procedures for accelerometers and gyroscopes are standardized by the *IEEE*, as outlined in (IEEE Standards Association, 2019) and (IEEE Standards Association, 2004), respectively.

4.1 Practical Considerations for Simplified Calibration

In cases where high-precision calibration is not required, such as in applications where IMU measurements are not the primary source of navigation data, simplified calibration procedures may be sufficient.

It is generally reasonable to assume that manufacturers ensure proper sensor alignment, meaning that individual sensing axes are mounted orthogonally to the sensor base. This assumption eliminates the need to explicitly model misalignment errors.

Similarly, in many applications, such as typical MAV flights, temperature variations during operation are minimal. This reduces the necessity of performing extensive temperature calibration. Furthermore, *g-sensitivity*, which refers to
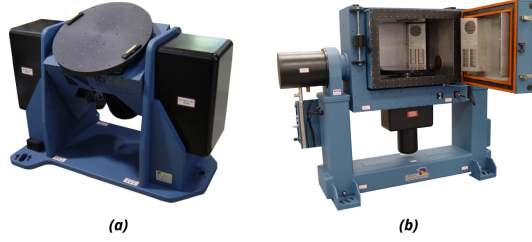
Figure 11: (a) Two-axis turntable and (b) Two-axis thermal chamber. *(Image source: vectornav.com)*

the effect of linear acceleration on gyroscope measurements, may be present but is often negligible in applications that do not involve extreme accelerations, such as missile guidance or high-dynamic maneuvers.

Under these assumptions, the primary calibration objectives are to determine sensor bias and scale factors. Additionally, stochastic errors, such as random noise, must be modeled appropriately. Gaussian distributions are often used due to their analytical convenience. In the context of Kalman filtering, Gaussian noise models are particularly advantageous since a Gaussian distribution remains Gaussian after undergoing a linear transformation, which is a fundamental property leveraged by Kalman filter algorithms.

4.2 Calibrated Sensor Measurements

In the previous section, the relationship between the ground truth acceleration and angular velocity and their corresponding measured quantities was established (Equations 11-12).

In a typical calibration scenario, the ground truth values are known, as the sensor is either placed in controlled static positions or moved in a predetermined manner. For instance, when the sensor is placed on a flat surface and remains stationary, the accelerometer should measure $+1g$ along the vertical axis, while the readings along the other axes should be zero. Similarly, the gyroscope measurements should be zero in all directions due to the absence of rotational motion. By systematically positioning the sensor on different faces, a dataset of controlled measurements can be collected. If a broader range of calibration data is required, a turntable can be employed to introduce controlled rotational motion.

Regardless of the calibration method used, estimating the sensor parameters requires solving an optimization problem. To formulate this problem, we invert Equations 11-12, obtaining the following expressions for the calibrated acceleration and angular velocity.

The ground truth acceleration is extracted by inverting the accelerometer noise model (Equation 11). This step isolates the true acceleration by compensating for systematic errors, such as bias and scaling distortions, resulting in a more reliable measurement for navigation and control applications.

$$\boldsymbol{a} = (\mathbf{I} + \boldsymbol{S}_a + \boldsymbol{M}_a)^{-1}(K_a\tilde{\boldsymbol{a}} - \boldsymbol{b}_a - \boldsymbol{T}_a\Delta T). \tag{15}$$

Similarly, by inverting the gyroscope noise model (Equation 12), the calibrated angular velocity is computed as

$$\boldsymbol{\omega} = (\mathbf{I} + \boldsymbol{S}_g + \boldsymbol{M}_g)^{-1}(K_g\tilde{\boldsymbol{\omega}} - \boldsymbol{b}_g - \boldsymbol{G}_g\boldsymbol{a} - \boldsymbol{T}_g\Delta T). \tag{16}$$

Using the simplified models given in Equations 13-14, the true acceleration and angular velocity can be estimated as follows:

$$\boldsymbol{\omega} = \tilde{\boldsymbol{\omega}} - \boldsymbol{b}_g, \tag{17}$$

$$\boldsymbol{a} = \tilde{\boldsymbol{a}} - \boldsymbol{b}_a. \tag{18}$$

These equations correct the raw sensor outputs by subtracting the estimated bias terms, providing a more accurate representation of the actual motion dynamics.

Since stochastic noise terms cannot be explicitly measured, they must be filtered out using estimation techniques such as Extended Kalman Filtering (EKF) or Unscented Kalman Filtering (UKF). These techniques refine sensor readings in real-time by estimating the underlying states while accounting for uncertainties, leading to improved measurement accuracy.

4.3   Solving for the Calibration Parameters

Upon collecting sufficient data, the error can be defined as:

$$e_a = \boldsymbol{a} - \tilde{\boldsymbol{a}}, \quad e_g = \boldsymbol{\omega} - \tilde{\boldsymbol{\omega}} \tag{19}$$

for the accelerometer and gyroscope, respectively.

Once these errors are established, the total error across all sample measurements is formulated as an optimization problem. By initializing the calibration parameters with some initial estimates, the optimization process seeks to minimize the error by determining the optimal calibration parameters.

For accelerometer calibration, the objective function is:

$$\underset{S_a, M_a, b_a, T_a}{\arg\min} \sum_i \|e_{a,i}\|^2. \tag{20}$$

Similarly, for gyroscope calibration, the objective function is:

$$\underset{S_g, M_g, b_g, G_g, T_g}{\arg\min} \sum_i \|e_{g,i}\|^2. \tag{21}$$

Various tools in the literature, such as the Ceres Solver and MATLAB toolboxes, can be used to solve these optimization problems efficiently (Agarwal, Mierle, & Others, 2012; The MathWorks, 2023).

5 CONCLUSION

IMUs are indispensable components of mobile robotic systems and play a critical role in various applications, including augmented reality headsets, autonomous vehicles, satellites, and missile guidance systems, among others.

Like any other sensor, IMUs are inherently noisy. Understanding their internal working principles is essential for any serious roboticist or engineer working in estimation and navigation. A thorough comprehension of these details allows one to interpret sensor measurements accurately and develop effective filtering and calibration techniques. Without proper handling of sensor noise and imperfections through appropriate mathematical models and calibration methods, system performance may degrade significantly, potentially leading to failure.

This work aims to provide an introduction to MEMS accelerometers and gyroscopes, covering their fundamental principles while leaving out many intricate details due to the vastness of the field and the limited scope of this document. Nevertheless, this document serves as a concise reference, highlighting the most crucial aspects of IMU modeling and calibration for practical applica-

tions.

References

Agarwal, S., Mierle, K., & Others. (2012). *Ceres solver.* (http://ceres-solver.org)

Bar-Itzhack, I. Y. (2000). New method for extracting the quaternion from a rotation matrix. *Journal of Guidance, Control, and Dynamics*, *23*, 1085-1087. doi: 10.2514/2.4654

Black, H. D. (1964). A passive system for determining the attitude of a satellite. *AIAA Journal*, *2*, 1350-1351. doi: 10.2514/3.2555

Bolton, W. (2003). *Mechatronics: electronic control systems in mechanical and electrical engineering*. Pearson Education.

Dantam, N. (2002). *Quaternion computation* (Tech. Rep.). Institute for Robotics and Intelligent Machines. Georgia Institute of Technology.

Eberly, D. (2002). *Quaternion algebra and calculus* (Tech. Rep.). Magic Software, Inc.

Euston, M., Coote, P., Mahony, R., Kim, J., & Hamel, T. (2008). A complementary filter for attitude estimation of a fixed-wing uav. In *2008 ieee/rsj international conference on intelligent robots and systems* (p. 340-345). IEEE. doi: 10.1109/IROS.2008.4650766

Fong, W., Ong, S., & Nee, A. (2008). Methods for in-field user calibration of an inertial measurement unit without external equipment. *Measurement Science and technology*, *19*(8), 085202.

Fourati, H., Manamanni, N., Afilal, L., & Handrich, Y. (2011). A nonlinear filtering approach for the attitude and dynamic body acceleration estimation based on inertial and magnetic sensors: Bio-logging application. *IEEE Sensors Journal*, *11*, 233-244. doi: 10.1109/JSEN .2010.2053353

Freescale, S. (2013). *Implementing a tilt-compensated ecompass using accelerometer and magnetometer sensors* (Tech. Rep.).

Greenheck, D. R. (2015). *Design and characterization of a low cost mems imu cluster for precision navigation* (Unpublished master's thesis). Marquette University.

Guo, S., Wu, J., Wang, Z., & Qian, J. (2017). Novel marg-sensor orientation estimation algorithm using fast kalman filter. *Journal of Sensors*, *2017*, 1-12. doi: 10.1155/2017/8542153

Hamel, T., & Mahony, R. (2006). Attitude estimation on so[3] based on direct inertial measurements. In *Proceedings 2006 ieee international conference on robotics and automation, 2006. icra 2006.* (p. 2170-2175). IEEE. doi: 10.1109/ROBOT.2006.1642025

Hartikainen, J., Solin, A., & Särkkä, S. (2011). *Optimal filtering with kalman filters and smoothers a manual for the matlab toolbox ekf/ukf* (Tech. Rep.).

Hartley, R., Trumpf, J., Dai, Y., & Li, H. (2013). Rotation averaging. *International Journal of Computer Vision*, *103*, 267-305. doi: 10.1007/s11263-012-0601-0

Huynh, D. Q. (2009). Metrics for 3d rotations: Comparison and analysis. *Journal of Mathematical Imaging and Vision*, *35*, 155-164. doi: 10.1007/s10851-009-0161-2

IEEE Standards Association. (2004). *IEEE Standard Specification Format Guide and Test Procedure for Coriolis Vibratory Gyros* (No. IEEE Std 1431-2004). IEEE. doi: 10.1109/IEEESTD.2004 .6543210

IEEE Standards Association. (2019). *IEEE Standard Specification Format Guide and Test Procedure for Linear Single-Axis, Nongyroscopic Accelerometers* (No. IEEE Std 1293-2018). IEEE. doi: 10.1109/IEEESTD.2019.1234567

Ioannou, G., Forti, N., Millefiori, L. M., Carniel, S., Renga, A., Tomasicchio, G., . . . Braca, P. (2024). Underwater inspection and monitoring: Technologies for autonomous operations.

IEEE Aerospace and Electronic Systems Magazine.

Katthöfer, D. I. K. G., & Yoon, I. Z. (2012). *Introduction into quaternions for spacecraft attitude representation* (Tech. Rep.).

Kraft, E. (2003). A quaternion-based unscented kalman filter for orientation tracking. In *Proceedings of the sixth international conference of information fusion* (Vol. 1, pp. 47–54).

Lam, Q., Stamatakos, N., Woodruff, C., & Ashton, S. (2003). Gyro modeling and estimation of its random noise sources. In *Aiaa guidance, navigation, and control conference and exhibit.* American Institute of Aeronautics and Astronautics. doi: 10.2514/6.2003-5562

LaValle, S. M., Yershova, A., Katsev, M., & Antonov, M. (2014). Head tracking for the oculus rift. In *2014 ieee international conference on robotics and automation (icra)* (pp. 187–194).

Liu, Z., Liu, W., Gong, X., & Wu, J. (2018). Simplified attitude determination algorithm using accelerometer and magnetometer with extremely low execution time. *Journal of Sensors*, *2018*, 1-11. doi: 10.1155/2018/8787236

Madgwick, S. O. H. (2010). *An efficient orientation filter for inertial and inertial/magnetic sensor arrays* (Tech. Rep.).

Mahony, R., Hamel, T., & Pflimlin, J.-M. (2005). Complementary filter design on the special orthogonal group so(3). In *Proceedings of the 44th ieee conference on decision and control* (p. 1477-1484). IEEE. doi: 10.1109/CDC.2005.1582367

Mahony, R., Hamel, T., & Pflimlin, J.-M. (2008). Nonlinear complementary filters on the special orthogonal group. *IEEE Transactions on Automatic Control*, *53*, 1203-1218. doi: 10.1109/TAC.2008.923738

Markley, F. L., Cheng, Y., Crassidis, J. L., & Oshman, Y. (2007). Averaging quaternions. *Journal of Guidance, Control, and Dynamics*, *30*, 1193-1197. doi: 10.2514/1.28949

Meier, L., Tanskanen, P., Fraundorfer, F., & Pollefeys, M. (2011). Pixhawk: A system for autonomous flight using onboard computer vision. In *2011 ieee international conference on robotics and automation* (pp. 2992–2997).

Michel, T., Geneves, P., Fourati, H., & Layaida, N. (2017). On attitude estimation with smartphones. In *2017 ieee international conference on pervasive computing and communications (percom)* (p. 267-275). IEEE. doi: 10.1109/PERCOM.2017.7917873

Özaslan, T., Loianno, G., Keller, J., Taylor, C. J., Kumar, V., Wozencraft, J. M., & Hood, T. (2017). Autonomous navigation and mapping for inspection of penstocks and tunnels with mavs. *IEEE Robotics and Automation Letters*, *2*(3), 1740–1747.

Rehder, J., Nikolic, J., Schneider, T., Hinzmann, T., & Siegwart, R. (2016). Extending kalibr: Calibrating the extrinsics of multiple imus and of individual axes. In *2016 ieee international conference on robotics and automation (icra)* (pp. 4304–4311).

Sun, K., Mohta, K., Pfrommer, B., Watterson, M., Liu, S., Mulgaonkar, Y., ... Kumar, V. (2018). Robust stereo visual inertial odometry for fast autonomous flight. *IEEE Robotics and Automation Letters*, *3*(2), 965–972.

Tedaldi, D., Pretto, A., & Menegatti, E. (2014). A robust and easy to implement method for imu calibration without external equipments. In *2014 ieee international conference on robotics and automation (icra)* (pp. 3042–3049).

The MathWorks, I. (2023). Sensor calibration toolbox [Computer software manual]. (https://www.mathworks.com/help/fusion/imu-calibration.html)

Valenti, R., Dryanovski, I., & Xiao, J. (2015). Keeping a good attitude: A quaternion-based orientation filter for imus and margs. *Sensors*, *15*, 19302-19330. doi: 10.3390/s150819302